JMEPEG (2018) 27:4444–4452
https://doi.org/10.1007/s11665-018-3577-2

1059-9495/$19.00

Novel Fabrication of a TiB_2 Grain Refiner and its Effect on Reducing Hot Tearing in AZ91D Magnesium Alloy

T.A. Davis and L. Bichler

(Submitted March 24, 2018; in revised form June 26, 2018; published online August 14, 2018)

Despite the increased use of magnesium (Mg) alloys in diverse engineering applications in recent years, further incorporation of complex Mg alloy castings remains challenging due to the alloy's relatively high susceptibility to hot tearing. A significant reduction in hot tearing via grain refinement was achieved in aluminum and ferrous alloys; however, an effective, long-lasting and inexpensive grain refiner for aluminum-containing Mg alloys remains elusive. In this work, a TiB_2 grain refiner was fabricated via a novel spark plasma sintering (SPS) powder metallurgy process. Then, its effectiveness in grain refining an AZ91D magnesium alloy was compared to that of a commercially available TiB_2 grain refiner produced by hot extrusion. Due to the homogeneous distribution of the $TiAl_3$ and TiB_2 particles in the grain refiner, as well as their effect on the alloy's microstructure evolution and solidification behavior, the SPS-TiB_2 grain refiner was observed to achieve a significant reduction in the grain size and hot tearing of the Al-containing AZ91D magnesium alloy.

Keywords AZ91D, grain refinement, hot tearing, magnesium

1. Introduction

The desire of product and materials designers to reduce component weight continues to drive the development of ultralight structural alloys. Magnesium (Mg) and its alloys offer significant weight savings compared to aluminum and steel alloys (Ref 1). With casting being the primary manufacturing route for shaping Mg alloy parts, fabrication of high-integrity defect-free components is paramount. Similar to other long freezing range alloys, cast Mg alloys are highly susceptible to hot tearing, which often leads to casting failure and undesirable casting scrap (Ref 2-5). Although hot tearing has been observed for decades and in many alloy systems, current methods for eliminating hot tears in the most industrially relevant magnesium alloys remain limited.

The microstructure of an alloy at high fractions of solid plays a key role on the alloy's hot tearing susceptibility (Ref 2, 4, 6-9). After the coherency point, interdendritic porosity may develop if liquid feeding is unable to accommodate solidification shrinkage. With continued solidification, the dendritic skeleton begins to experience non-uniform stress (due to the 3D casting geometry, as well as porosity-induced stress concentrations), potentially leading to dendrite fracture and the nucleation of a hot tear (Ref 8, 9). In shape castings, where the alloy is constrained by the surrounding rigid mold, hot tearing is often accelerated by the casting's geometric factors, such as sharp features or section-thickness transitions (Ref 3, 6, 10). The formed hot tears subsequently propagate through the interdendritic regions, where eutectic liquid is still present at the end of solidification, leading to a fracture resembling liquid metal embrittlement. There have been many attempts to prevent hot tearing in many alloy systems. For example, optimizing the pouring and mold temperatures, alloy composition, introducing additives, chills, and other methods have been investigated, but many of these techniques were difficult or costly to adopt on an industrial scale (Ref 3, 11, 12).

New attempts of reducing hot tearing via microstructural engineering approach have been recently reported. For example, grain refinement was shown to have a significant impact on the reduction in hot tear severity in several alloy systems (Ref 5, 10, 13-16). With smaller grains, the eutectic liquid mobility improved and the stress experienced by individual grains was reduced (Ref 10, 17). Currently, grain refiners for aluminum (Al)-containing magnesium alloys, which constitute the majority of industrially relevant Mg alloys, show poor grain refining ability, due to the undesirable reactions between Al present in the alloy and the grain refiner. Further, the uniform distribution of the refining particles in the liquid alloy is often challenging, due to particle flotation or settling during liquid metal treatment.

An aluminum-titanium-boride (Al-Ti-B) grain refiner (also called TiBor) has been successfully used for the treatment of complex aluminum alloys. This commercially available grain refiner is typically produced via halide salt reactions, followed by hot extrusion into rods. However, this manufacturing process offers a limited control over the distribution of the refining particles in the extruded rod. Further, the suitability of Al grain refiners for Al-containing Mg alloys has not been investigated in detail. Initial experiments by Elsayed (Ref 10) and Chen (Ref 18) on Al-Ti-B refiners revealed some success with grain refinement of Mg alloys, but an in-depth defect analysis was not performed. In the case of the Al-5Ti-1B refiner, grain refinement was speculated to be the result of heterogeneous nucleation and grain growth restriction. Chen (Ref 18) also suggested that both mechanisms would be hindered if a grain refiner particle agglomeration would occur. Chen reported that when the TiBor grain refiner was added to the Mg alloy, an $TiAl_3$ phase formed, but readily dissolved and produced Ti, which in turn facilitated α-Mg growth restriction.

T.A. Davis and **L. Bichler**, School of Engineering, University of British Columbia – Okanagan, 3333 University Way, Kelowna V1V 1V7, Canada. Contact e-mail: lukas.bichler@ubc.ca.

However, Elsayed (Ref 10) observed intact and unreacted $TiAl_3$ particles in the as-cast Mg alloys, suggesting the grain refining particles were stable during solidification and could potentially serve as nucleating substrate for the α-Mg phase. Therefore, the exact mechanism of grain refinement due to the TiB_2 or $TiAl_3$ remains unclear. Additionally, recent studies suggest that Al-Ti-B grain refiners may be ineffective in AZ91Mg alloys (Ref 19). The formation of Al-Mn phase around the refining particles poisons their ability to serve as an effective nucleation site.

In the present work, a novel method to fabricate a grain refiner was explored. An Al-Ti-B grain refiner was fabricated using the spark plasma sintering (SPS) powder metallurgy route. Then, the refiner was added into liquid AZ91D magnesium alloy during casting trials. Similarly, the commercially available Al-Ti-B grain refiner was also used during casting trials, and its grain refinement potency was compared to the SPS prepared Al-Ti-B refiner.

In addition to examining the resulting as-cast microstructure of the refined AZ91D magnesium alloy, the effect of the grain refiners on the hot tearing susceptibility of the AZ91D alloy was quantitatively studied with a mold instrumented with thermocouples and a load cell, thus enabling an in situ analysis of casting solidification and hot tear formation.

2. Experimental Procedure

2.1 Experimental Setup

A steel mold instrumented with a load cell and thermocouples (developed by Zhen and Hort) was used for all experiments in this work. Prior work with the mold, its design and limitations can be found in the literature (Ref 5, 6, 12, 17).

The mold had a vertical downsprue, connected to a single horizontal bar ~ 10 mm in diameter, oriented at 90° to the downsprue. The opposite end of the horizontal bar was connected to a load cell (Omega, LC101-250) via a threaded bar, thus enabling the measurement of the shrinkage force of the horizontal bar during its solidification. Also, a 0.5-mm-diameter thermocouple (Omega, TJ36-CASS-020E-24) was inserted into the mold cavity at the 90° junction, coinciding with the region where hot tears readily nucleated (since this region posed a geometrical stress concentration). The force and temperature were collected during casting solidification with a data acquisition unit (Omega, OMB-DAQ-56) operating at 2 Hz. To control the solidification rate and the severity of hot tears, the mold temperature was adjusted between 25 and 400 °C with electrical heaters.

2.2 Grain Refiner Manufacturing

A novel grain refiner was fabricated at the spark plasma sintering laboratory at the University of British Columbia, Okanagan campus, Kelowna, Canada. The refiner consisted of a micron-scale Al powder (Alfa Aesar, 11067) blended with $TiAl_3$ (Alfa Aesar, 22895) and TiB_2 (Sigma-Aldrich, 336289) powders. In order to sinter the grain refiner, the weight percentage of the Al, $TiAl_3$, and TiB_2 powders was weighed to yield an equivalent of the commercially available Al-5Ti-1B "TiBor" grain refiner (Ref 5, 10, 18-20). Before SPS processing, the powder blend was homogenized in a planetary ball mill (Fritsch Pulverisette 7) in MeOH. Pressureless sintering at 450 °C was carried out to consolidate the powder blends into a 20-mm (diam.) pellet approximately 5 mm thick.

2.3 Casting Parameters

Previous work by the authors revealed that the onset of hot tearing for the AZ91D magnesium alloy poured at 720 °C occurred at 325 °C mold temperature (Ref 5). Therefore, all casting trails were performed at these pouring and mold temperatures and three replicates were made for each alloy composition and grain refinement level. During melting and casting, the AZ91D alloy was protected with CO_2 gas to avoid melt oxidation.

Approximately 500 g of AZ91D was melted in an electric resistance furnace in a 1020 steel crucible. When the melt reached 740 °C, 0.1 wt.% addition of a grain refiner was manually stirred into the melt. After stirring for 30 s, the melt was held for 2 min, after which the melt was removed from the furnace and poured at 720 °C.

Three alloys with refinement conditions were investigated in this work:

(1) Unrefined AZ91D alloy
(2) AZ91D alloy refined with a commercially available Ti-Bor (referred to as "COM-TiBor")
(3) AZ91D alloy refined with a spark plasma-sintered TiBor (referred to as "SPS-TiBor").

2.4 Material Characterization

The microstructure near the 90° corner of the casting (i.e., region where hot tears were observed) was examined using a Ziess Axiovert A1m inverted optical microscope coupled with a Buehler OmniMet image analysis software. The grain size of the as-cast alloy was measured via the linear intercept method [ASTM E112-13 standard (Ref 21)]. The values of average grain size reported in this work represent grain measurements at the central region of the horizontal bar's cross section (i.e., ultrafine grains at the metal-mold interface were not included in the grain size measurements). The grain size through the critical region was measured at five locations and averaged. Scanning electron microscopy (SEM) combined with x-ray energy dispersive spectroscopy (XEDS) was used for chemical analysis of precipitates and the matrix. Hardness was measured using a Vickers digital microhardness tester (Buehler, Wilson VH3100 Vickers and Knoop hardness tester). A minimum of 30 measurements were performed on a 3 mm by 10 mm grid, with a 0.2-kg load and a 15 s dwell time for each measurement.

3. Results and Discussion

3.1 Characterization of Raw Grain Refiners

Figure 1 shows SEM micrographs of the as-received COM-TiBor and the manufactured SPS-TiBor refiners at various magnifications. Both grain refiners had the $TiAl_3$ and TiB_2 particles dispersed throughout the Al matrix. However, the homogeneity of the particle dispersion varied for the COM-TiBor and the SPS-TiBor.

In both refiners, the large white cuboidal particles (avg. size ~ 40 μm) were the $TiAl_3$ phase. In the case of the SPS

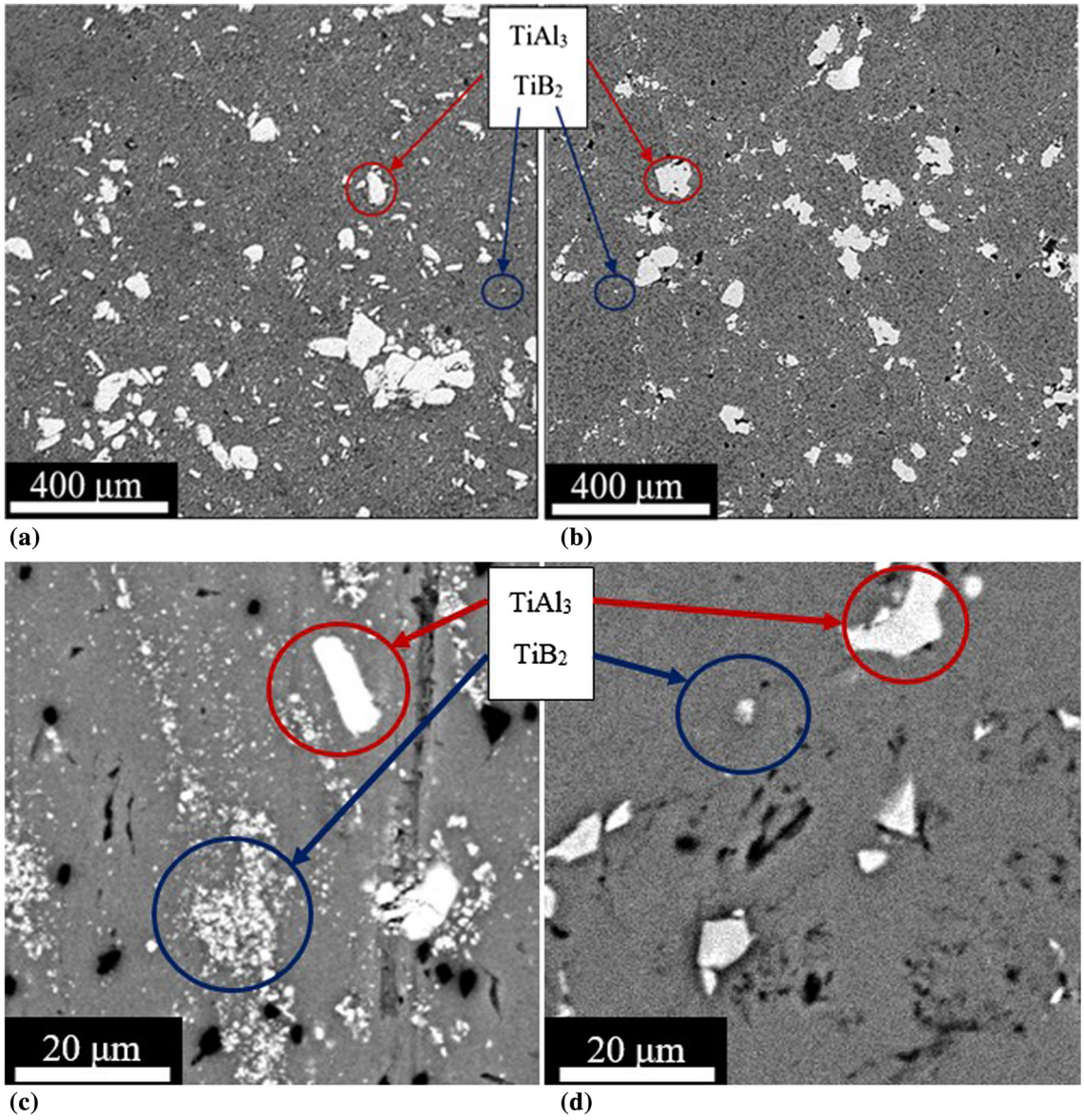

Fig. 1 SEM micrographs of grain refiners; (a) COM-TiBor refiner 400×, (b) SPS-TiBor refiner 400×, (c) COM-TiBor refiner 4000×, and (d) SPS-TiBor refiner 4000×

grain refiner, the distribution of these $TiAl_3$ particles was more uniform throughout the entire grain refiner, with a reduced interlocking and agglomeration. Also, both grain refiners had clearly visible TiB_2 particles, as shown in Fig. 2(c) and (d). A similar microstructure of the commercial TiBor was reported in the literature (Ref 10, 18). However, in the SPS refiner, fine TiB_2 particles were dispersed throughout the microstructure, while in the commercial refiner, the TiB_2 particles appeared to agglomerate near the $TiAl_3$ particles, as seen in Fig. 2(c). With respect to the TiB_2 particles, the literature suggests that despite their presence in the commercial refiner, their refining efficiency rapidly deteriorates if they agglomerate (Ref 18, 20).

Figure 2 shows the TiB_2 and $TiAl_3$ particles, along with the results of XEDS linescan chemical analysis across the $TiAl_3$ particles in the grain refiners. The linescans suggest that in the COM-TiBor, the Al content decreased rapidly at the $TiAl_3$-Al (matrix) interface, while in the case of the SPS-TiBor, the Al content decreased gradually. Similar linescan analysis was not possible for the TiB_2 particles due to their size. Thus, the XEDS linescan results suggest that during SPS processing, the electric discharge between the Al powder matrix and the $TiAl_3$ (and likely TiB_2) particles enabled enhanced interdiffusion at the grain refining particle's interface. This is seen in Fig. 2(b), where a dark-gray region was seen on the periphery of the $TiAl_3$ particle. Consequently, the SPS process facilitated diffusion-driven surface modification of the reinforcing particles, which could significantly enhance the wettability of liquid Mg on the refining particles after the addition of the grain refiner into the liquid AZ91D magnesium alloy (Ref 22). The combined effect of enhanced wetting, as well as a more uniform distribution of TiB_2 and $TiAl_3$ throughout the grain refiner likely enhanced heterogenous nucleation of the α-Mg phase during solidification, as discussed in following sections.

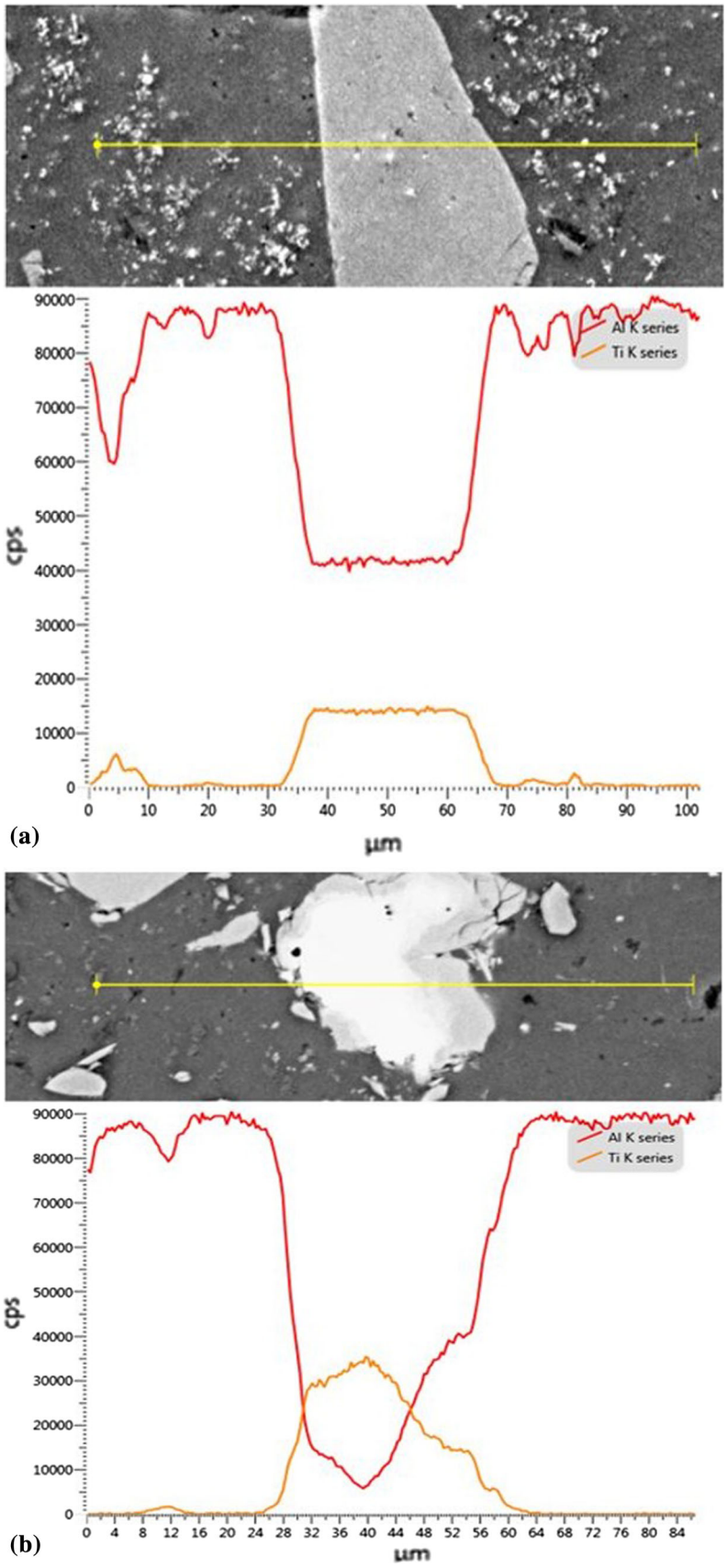

Fig. 2 SEM images and XEDS linescan data of $TiAl_3$ particle, red line denotes Al and orange line denotes Ti; (a) commercial refiner, (b) SPS refiner (Color figure online)

3.2 Microstructure of Grain-Refined AZ91D Castings

The effect of the grain refiner additions on the as-cast grain structure of the AZ91D magnesium alloy is illustrated in Fig. 3. As seen in Table 1, in the case of the SPS-TiBor grain refiner, the grain diameter reduced by ~ 80%, while for the COM-TiBor, the grain diameter reduced by ~ 46%. Also, the SPS-TiBor-refined casting had a significantly more homogeneous grain structure, as observed by the grain size standard deviation. The TiB_2 and $TiAl_3$ particles were not located within the as-cast AZ91D alloy casting during SEM analysis due to the overall low grain refiner addition level (i.e., only 0.1 wt.%) and also their relative size.

With a finer grain size observed in the refined alloy in Fig. 3, the homogeneity of the interdendritic eutectic β-$Mg_{17}Al_{12}$ phase was observed to increase. The SPS-TiBor refiner dispersed the eutectic phase throughout the microstructure, as seen in Fig. 3(c). With this low-melting-temperature eutectic phase being distributed on the grain boundaries, it is expected that intergranular feeding at the end of solidification was improved in the SPS-TiBor-refined casting. Such enhanced feeding would enable grain sliding and a concomitant reduction in evolving stresses and strains during casting solidification. This would have a direct impact on the hot tearing severity of the alloy.

Figure 4 shows the grain size variation in the horizontal bar at the critical hot tear region (i.e., at the junction of the downsprue and the horizontal bar). The grains were measured from the top surface to the bottom surface of the horizontal bar. The unrefined AZ91D showed a large variation of grain size between the metal–mold interface (i.e., "top" and "bottom" locations) and the centerpoint of the horizontal bar. These measurements suggest a lack of heterogenous nucleation throughout the horizontal bar. Further, the center region of this casting showed a significantly higher grain size, thus suggesting that the grains were allowed to grow possibly due to the lower cooling rate in the horizontal bar center region, or due to the reduced grain impingement during solidification. The COM-TiBor-refined alloy showed a similar trend in the variation of the grain size, despite achieving an overall lower grain size reduction. In contrast, the SPS-TiBor-refined alloy had a consistent grain size throughout the entire horizontal bar. This result suggests that the SPS-TiBor addition resulted in a faster and uniform heterogeneous nucleation of the α-Mg throughout the casting. This effect was more dominant on the grain size than the variation of the cooling rate. A similar effect has been reported by the authors earlier, where a refinement

Table 1 Average grain size

Alloy	Grain size (Avg. ± std. dev., μm)
Unrefined AZ91D	275 ± 80
AZ91D + COM-TiBor	155 ± 22
AZ91D + SPS-TiBor	65 ± 5

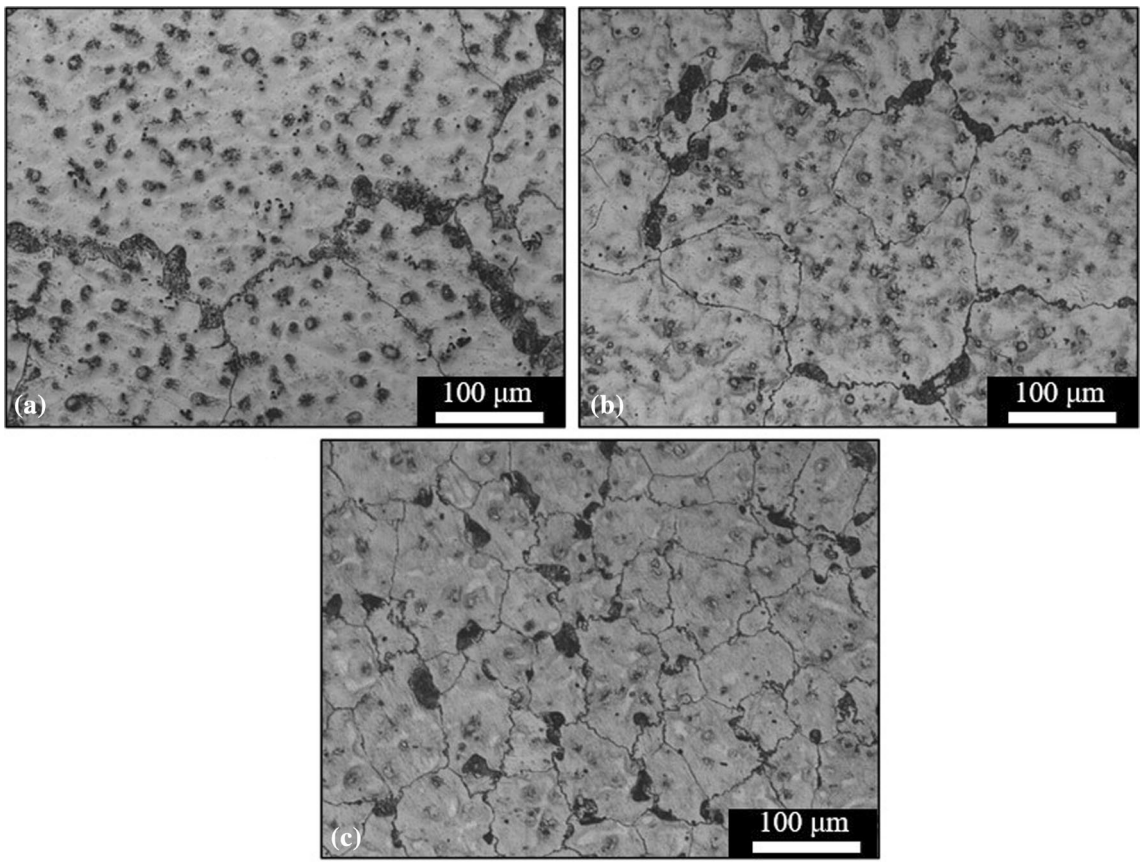

Fig. 3 As-cast microstructure of AZ91D castings (200× magnification): (a) unrefined AZ91D alloy, (b) AZ91D + COM-TiBor alloy, and (c) AZ91D + SPS-TiBor alloy

with SPS-processed additives also resulted in a consistent grain size throughout the casting (Ref 5).

3.3 Hot Tear Severity

The hot tear severity of each casting was analyzed by sectioning through the critical region of the casting to reveal the depth of the hot tears. Figure 5 shows representative micrographs of the castings near the 90º junction of the casting's downsprue and the horizontal bar.

In the case of the unrefined AZ91D alloy, the length of the tear (Fig. 5a) was ~ 0.8-1.0 mm. Although the COM-TiBor casting achieved grain refinement, it did not yield a significant hot tear reduction, as seen in Fig. 5(b), where the hot tear was ~ 0.8 mm long. In the case of the SPS-TiBor grain-refined casting, the hot tear virtually disappeared, and only a surface porosity spanning two grains was detected.

A similar trend was noted in the literature (Ref 10) when AZ91E alloy was used during sand casting and was treated with two Al-Ti-B-based grain refiners. Despite producing a limited degree of grain refinement, the hot tearing severity was not observed to be proportional to the level of grain refinement. The hot tear severity and grain size measurements suggest hot tearing is not only dependent on the grain size and the presence of a stress concentration, but also on the thermal- and solidification-induced strain, distribution of eutectic liquid, and grain homogeneity.

3.4 Cooling and Load Curve Analysis

Representative cooling and load in situ data obtained during casting solidification are provided in Fig. 6. The trends in the present work are consistent with general trends reported in the literature for the mold setup (Ref 12, 23, 24).

As observed in Fig. 6, a rapid force increase was recorded by the load cell after filling of the mold. This initial rapid increase has been associated with the formation of a solid skin at the casting–mold interface, as well as the formation of a

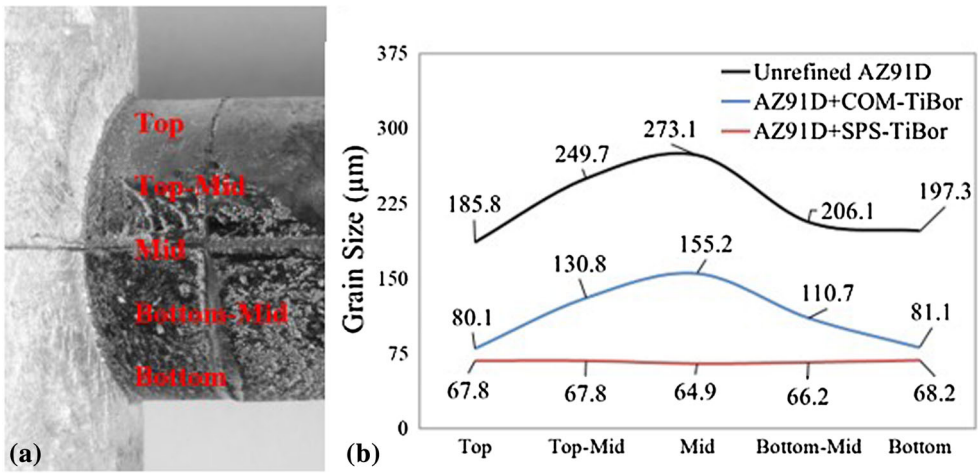

Fig. 4 Variation of grain size through the cross section at the critical hot tear location for each casting; (a) measurement locations and (b) measurements

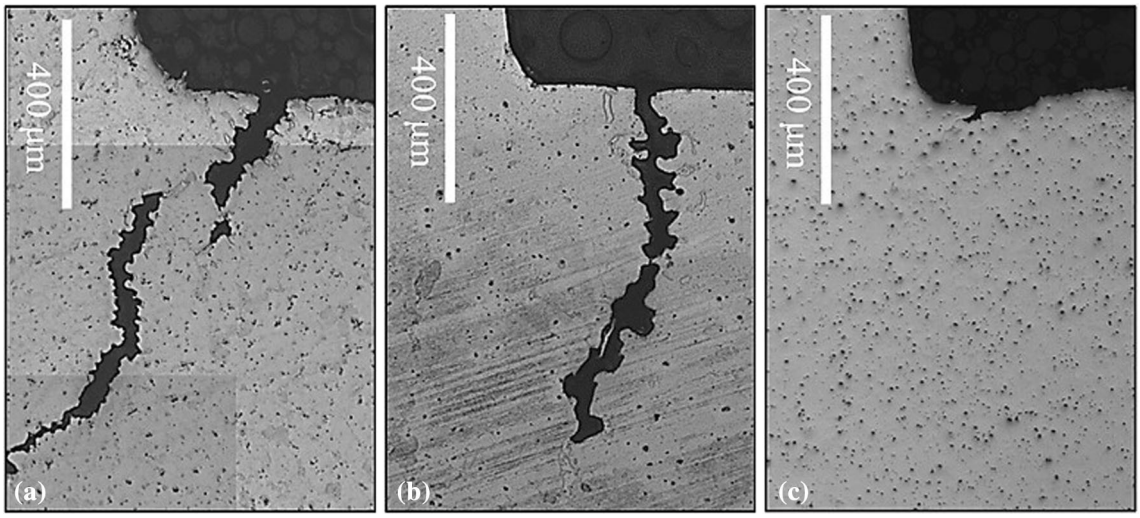

Fig. 5 Hot tear severity in the critical region; (a) unrefined AZ91D alloy, (b) AZ91D + COM-TiBor alloy, and (c) AZ91D + SPS-TiBor alloy

dendritic skeleton in the semisolid alloy. Formation of this solid phase would enable load transfer through the solidifying alloy to the load cell.

At ~ 10-20 s, a large inflection in the load and cooling curves was noted. Since the alloy was mostly solid at this time (> ~0 .85 solid fraction), this inflection has been associated with a contracting dendritic structure and interdendritic feeding counteracting this contraction (Ref 12, 17). At the end of solidification, Fig. 6(a) reveals that for the unrefined AZ91D and AZ91D + COM-TiBor alloys, a force relaxation was recorded (a dip in the curve). This relaxation has been associated with the opening of a hot tear. In the case of the AZ91D + SPS-TiBor alloy, no force relaxation was noted.

The solidification temperature range was comparable for all alloys, as seen in Table 2; however, the rates of solidification varied significantly with the addition of the different grain refiners. The increase in the cooling rate in the SPS-TiBor grain-refined casting was possibly caused by several factors. First, the increased number of effective nucleation sites would result in a faster latent heat release during the early stages of solidification. Second, with effective heterogeneous nucleation and faster solid fraction development (Fig. 6c), dendrite coherency was achieved sooner in the SPS-TiBor-refined casting. As a result, due to the higher fraction of solid, the heat extraction from the casting via conduction to the surrounding steel mold was higher in the SPS-TiBor casting

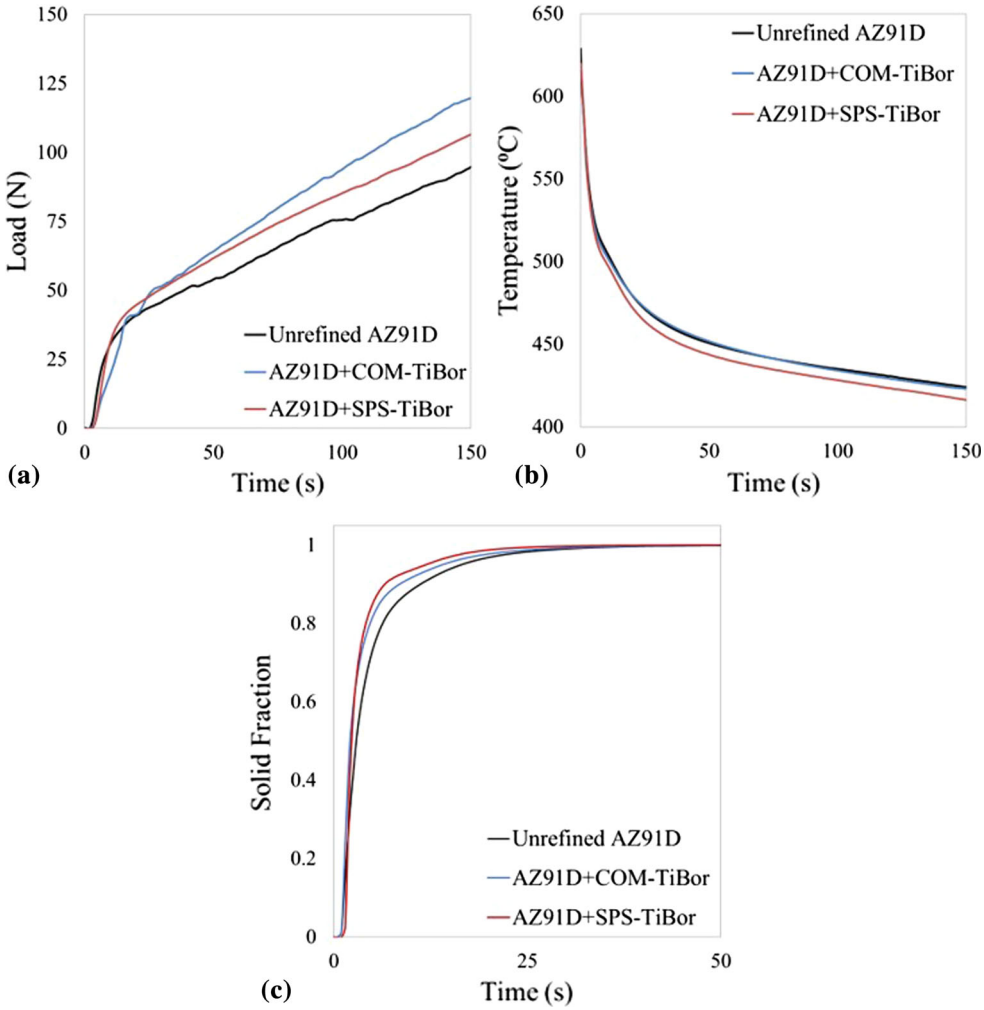

Fig. 6 In situ load and temperature data for unrefined AZ91D alloy, AZ91D + COM-TiBor alloy, and AZ91D + SPS-TiBor alloy (dotted lines represent first derivative); (a) load curves, (b) temperature curves, and (c) solid fraction curves

Table 2 Temperature/solidification data

Alloy	T-liquidus, °C	T-solidus, °C	Freezing range, °C	Total solidification time, s	Average cooling rate, °C/s
Unrefined AZ91D	594.7	430.3	164.4	120	1.3
AZ91D +COM-TiBor	595.2	429.8	165.4	102.5	1.6
AZ91D + SPS-TiBor	596.8	432.2	164.6	72	2.3

Table 3 Load data

Alloy	Load at the inflection, N	Load at end of solidification, N	Duration of semisolid period after load inflection, s
Unrefined AZ91D	21.4	81.1	113.5
AZ91D + COM-TiBor	14.4	93.2	94.5
AZ91D + SPS-TiBor	31.2	75.2	62

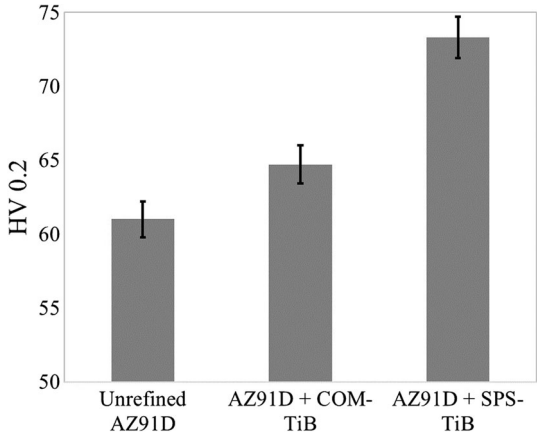

Fig. 7 Hardness of studied alloys

than in the unrefined or COM-TiBor-refined castings, where a semisolid alloy remained in the center region of the horizontal bar for a longer period of time.

The results in Table 3 further support the microstructure analysis and suggest that the formation of grains in the SPS-TiBor-refined alloy was rapid. Consequently, the eutectic phase was forced to disperse at the grain boundaries within a shorter period than in the remaining two alloys. As a result, the possibility of a continuous eutectic liquid path facilitating solidification shrinkage healing at the end of solidification likely increased, resulting in lower porosity and hot tear severity, as seen in Fig. 5(c).

An analysis of the load evolution (Table 3) suggests that at the first load inflection at $\sim$ 10-20 s, the SPS-TiBor-refined alloy had developed the highest load. Despite this high loading, however, the dendritic structure of the alloy was most evolved (Fig. 6c), thus being capable of sustaining and redistributing solidification stress during this stage of solidification. After this point, the AZ91D + SPS-TiBor alloy spent less time as semisolid during the late stages of solidification when hot tearing generally occurs (Ref 6, 7).

3.5 Microhardness Results

The results of Vickers microhardness of the three alloys are shown in Fig. 7. As expected, a reduced grain size in the grain-refined alloys enhanced the hardness in comparison to the unrefined AZ91D alloy.

The average hardness of the unrefined casting was 61.0 HV 0.2, which is in agreement with published values for permanent mold-cast AZ91D alloy (Ref 1, 18). The hardness increase due to refinement from the COM-TiBor addition was 6% (64.7 HV0.2), while for the SPS-TiBor alloy the hardness increased by $\sim$ 20% (73.3 HV0.2). These results are consistent with the grain size analysis discussed earlier. In addition to a finer grain size, however, the improvement of hardness in the SPS-TiBor alloy casting likely came from the well-dispersed hard and brittle β-$Mg_{17}Al_{12}$ phase along the grain boundaries.

4. Conclusions

The results of this work reveal that the distribution of the grain refining particles in a grain refiner may play a key role in the ability to treat difficult-to-refine alloys, such as the AZ91D magnesium alloy. The commercially available grain refiner, although providing a grain refinement, was not as effective as spark plasma-sintered grain refiner with uniformly dispersed grain refining particles.

- The SPS-TiB refiner reduced the grain size of AZ91D magnesium alloy by additional 25% in comparison with the commercial grain refiner. This was attributed to a better particle distribution and enhanced wetting and diffusion of Al on the refining particles, leading to improved heterogenous nucleation of α-Mg during AZ91D's solidification.
- While the commercial grain refiner did not significantly impact hot tearing, the SPS refiner eliminated hot tears due to improved interdendritic feeding, smaller grain size, and associated stress homogenization.
- The effective nucleation in the SPS-TiBor-treated casting resulted in the alloy's ability to sustain solidification stress, without forming a hot tear.

Acknowledgments

The authors would like to acknowledge the financial support from the NSERC Discovery grant. The authors would also like to acknowledge the support from Dr. Norbert Hort and the Magnesium Innovation Centre, Helmholtz-Zentrum in Geesthacht, Germany.

Raw Data Availability

The raw data required to reproduce these findings cannot be shared in full at this time as the data also form a part of an ongoing study and a Doctoral dissertation of Mr. T. Davis.

References

1. M. Avedesian and H. Baker, *Magnesium and Magnesium Alloys*, ASM International, Materials Park, 1999
2. Y. Wang, B. Sun, Q. Wang, Y. Zhu, and W. Ding, An Understanding of the Hot Tearing Mechanism in AZ91 Magnesium Alloy, *Mater. Lett.*, 2002, **53**(1-2), p 35–39
3. H. Huang, P.H. Fu, Y.X. Wang, L.M. Peng, and H.Y. Jiang, Effect of Pouring and Mold Temperatures on Hot Tearing Susceptibility of AZ91D and Mg-3Nd-0.2Zn-Zr Mg Alloys, *Trans. Nonferrous Met. Soc. China (English Ed.)*, 2014, **24**(4), p 922–929
4. L. Bichler, A. Elsayed, K. Lee, and C. Ravindran, Influence of Mold and Pouring Temperatures on Hot Tearing Susceptibility of AZ91D Magnesium Alloy, *Int. J. Met.*, 2008, **2**(1), p 43–54

5. T.A. Davis, L. Bichler, F. D'Elia, and N. Hort, Effect of TiBor on the Grain Refinement and Hot Tearing Susceptibility of AZ91D Magnesium Alloy, *J. Alloys Compd.*, 2018, **759**, p 70–79
6. Y.D. Huang, Z. Wang, A. Srinivasan, K.U. Kainer, and N. Hort, Metallurgical Characterization of Hot Tearing Curves Recorded During Solidification of Magnesium Alloys, *Acta Phys. Pol. A*, 2012, **122**(3), p 497–500
7. J. Song, F. Pan, B. Jiang, A. Atrens, M.X. Zhang, and Y. Lu, A Review on Hot Tearing of Magnesium Alloys, *J. Magnes. Alloy*, 2016, **4**(3), p 151–172
8. D.G. Eskin and L. Katgerman, A Quest for a New Hot Tearing Criterion, *Metall. Mater. Trans. A*, 2007, **38A**(7), p 1511–1519
9. M. Rappaz, J.M. Drezet, and M. Gremaud, A New Hot-Tearing Criterion, *Metall. Mater. Trans. A*, 1999, **30**(2), p 449–455
10. A. Elsayed, *Novel Grain Refinement of AZ91E Magnesium Alloy and the Effect on Hot Tearing During Solidfication*, Ryerson University, Canada, 2010
11. Z. Ning, P. Cao, H. Wang, J. Sun, and D. Liu, Effect of Cooling Conditions on Grain Size of AZ91 Alloy, *J. Mater. Sci. Technol.*, 2007, **23**(5), p 645–649
12. Z.S. Zhen, N. Hort, Y.D. Huang, O. Utke, N. Petri, and K.U. Kainer, Hot Tearing Behaviour of Binary Mg-1Al Alloy Using a Contraction Force Measuring Method, *Int. J. Cast Met. Res.*, 2009, **22**(1–4), p 331–334
13. A.M. Nabawy, A.M. Samuel, F.H. Samuel, and H.W. Doty, Effects of Grain Refiner Additions (Zr, Ti–B) and of Mould Variables on Hot Tearing Susceptibility of Recently Developed Al-2wt.%Cu alloy, *Int. J. Cast Met. Res.*, 2013, **26**(5), p 308–317
14. T.J. Chen, X.D. Jiang, Y. Ma, R.Q. Wang, and Y. Hao, Grain Refinement of AZ91D Magnesium Alloy by $MgCO_3$, *Mater. Res.*, 2011, **14**(1), p 124–133
15. T.J. Chen, X.D. Jiang, Y. Ma, Y.D. Li, and Y. Hao, Grain Refinement of AZ91D Magnesium Alloy by SiC, *J. Alloys Compd.*, 2010, **496**(1–2), p 218–225
16. D.H. StJohn, M. Qian, M.A. Easton, P. Cao, and Z. Hildebrand, Grain Refinement of Magnesium Alloys, *Metall. Mater. Trans. A*, 2005, **36**(7), p 1669–1679
17. L. Zhou, Y.D. Huang, P.L. Mao, K.U. Kainer, Z. Liu, and N. Hort, Influence of Composition on Hot Tearing in Binary Mg-Zn Alloys, *Int. J. Cast Met. Res.*, 2011, **24**(3–4), p 170–176
18. T.J. Chen, R.Q. Wang, Y. Ma, and Y. Hao, Grain Refinement of AZ91D Magnesium Alloy by Al-Ti-B Master Alloy and its Effect on Mechanical Properties, *Mater. Des.*, 2012, **34**, p 637–648
19. A. Koltygin, V. Bazhenov, and U. Mahmadiyorov, Influence of Al-5Ti-1B Master Alloy Addition on the Grain Size of AZ91 Alloy, *J. Magnes. Alloy*, 2017, **5**(3), p 313–319
20. M. Vlasceanu, S. Lun Sin, A. Elsayed, and C. Ravindran, Effect of Al-5Ti-1B on Grain Refinement, Dendrite Coherency and Porosity of AZ91E Magnesium Alloy, *Int. J. Cast Met. Res.*, 2015, **28**(1), p 39–46
21. Astm Standard, E112-12: Standard Test Methods for Determining Average Grain Size, *ASTM Int.*, 2012, **E112–12**, p 1–27
22. N. Eustathopoulos, Wetting by Liquid Metals—Application in Materials Processing: The Contribution of the Grenoble Group, *Metals (Basel)*, 2015, **5**(1), p 350–370
23. A. Srinivasan, Z. Wang, Y. Huang, F. Beckmann, K.U. Kainer, and N. Hort, Hot Tearing Characteristics of Binary Mg-Gd Alloy Castings, *Metall. Mater. Trans. A Phys. Metall. Mater. Sci.*, 2013, **44**(5), p 2285–2298
24. Z. Wang et al., Experimental and Numerical Analysis of Hot Tearing Susceptibility for Mg-Y Alloys, *J. Mater. Sci.*, 2014, **49**(1), p 353–362